Evaluation of the Photosynthetic Reaction Center Protein for Potential Use as a Bioelectronic Circuit Element

ARTICLE *in* BIOTECHNOLOGY PROGRESS · JULY 2007

Impact Factor: 2.15 · DOI: 10.1021/bp070042s · Source: PubMed

3 AUTHORS, INCLUDING:

Deborah K Hanson
Argonne National Laboratory
77 PUBLICATIONS **2,014** CITATIONS
SEE PROFILE

Millicent anne Firestone
University of Chicago
100 PUBLICATIONS **2,078** CITATIONS
SEE PROFILE

Evaluation of the Photosynthetic Reaction Center Protein for Potential Use as a Bioelectronic Circuit Element

Brian D. Reiss,[†,‡] Deborah K. Hanson,[§] and Millicent A. Firestone*[,†]

Materials Science and Biosciences Divisions, Argonne National Laboratory, 9700 South Cass Avenue, Argonne, Illinois 60439

The characterization of a bioelectronic composite prepared by molecular wiring of a bacterial photosynthetic reaction center (RC) to a metal (Au) electrode is described. Two unique attachment sites on the protein surface were studied as sites for electrical connections—a polyhistidine tag introduced by site-directed mutagenesis and a native cysteine amino acid residue. These two attachment sites were evaluated independently and found to serve effectively in coupling the protein to the electrode surface asymmetrically. Cyclic voltammetry (CV) was used to monitor protein integrity and confirm protein chemisorption and orientation to the organofunctionalized gold electrode. Single-protein transport measurements made with conductive atomic force microscopy (C-AFM) were used to study the electrical transport. Current−voltage ($I-V$) curves obtained by wiring the protein at the polyhistidine tag showed diodelike behavior. The cysteine attachment site does not serve as an efficient means to address the protein electrically. Scanning tunneling spectroscopy (STS) performed on RCs coupled at the donor side under both dark- and white-light-illuminated conditions confirmed the C-AFM studies.

Introduction

During billions of years of evolution, Nature has perfected proteins structurally and functionally to perform a wide array of functions, including energy conversion, transportation, and information processing (signaling). The use of biological entities such as proteins as core components in the fabrication of hybrid materials remains as one of the grand challenges in nanoscience (*1*). Examples of such biological entities are proteins derived from photosynthetic systems which convert solar energy into biochemical energy in plants, algae, and photosynthetic bacteria. There has been recent interest in studying the means by which to incorporate photosynthetic proteins into electronic devices for generating photocurrent (*2*−*5*). The reaction center (RC) from purple non-sulfur bacteria is the simplest and most well-studied of the photosynthetic proteins (*6*). The RC, such as that from *Rhodobacter* (*R.*) *sphaeroides*, is responsible for the first step in conversion of light energy into a transmembrane, charge-separated state and is a large integral membrane protein assembly composed of two hydrophobic (L and M) subunits and one hydrophilic (H) subunit (Figure 1a). The photochemically active cofactors are bound noncovalently within the L and M subunits and are arranged in two symmetric branches designated A and B (Figure 1a). The light-induced electron-transfer cycle is initiated by excitation of the bacteriochlorophyll dimer (special pair), P. An electron is then transferred sequentially through only the right (A) branch of the cofactor chain to a bacteriopheophytin, H_A (via monomeric bacteriochlorophyll B_A), followed by transfer to a ubiquinone, Q_A. The electron is then transferred from Q_A to Q_B, converting it into a semiquinone radical. In Nature, the electron-transfer cycle, that is the oxidation/reduction of Q_B^-/P^+, is completed by the presence of other proteins (membrane-bound and soluble cytochromes). The electron-transfer properties of the RC equate to current moving through the protein, and thus the RC could be used as the basis for fabrication of a nanoscale bioinorganic optoelectronic or photovoltaic device.

To adapt RCs as the basis for such a device, three general material challenges must be addressed: stabilization of the protein outside its native biomembrane, unidirectional orientation of the protein, and efficient means to couple the internal electron-transfer cycle to an external electrode system. In this work, we describe an approach to both asymmetrically orient and wire the RC to a conventional, inorganic (gold) electrode, and we evaluate the electron transport properties of these bioinorganic composites.

Materials and Methods

Donor-Side Wiring of RCs. Briefly, Ni^{2+}−nitrilotriacetic acid functionalized (Ni−NTA-functionalized) Au electrodes (50 nm thick prepared by thermal evaporation on mercaptopropyl-silane-modified glass slides) were prepared in four steps. First, Au films were immersed in a methanolic solution of 0.1 M mercaptoethylamine for 2 h at room temperature, yielding an amine-terminated surface, which was then rinsed in methanol and reacted with a 25 mM 1,4-phenylene diisothiocyanate (25 mM) solution in dimethylformamide and was finally rinsed in acetone. The coupling of the NTA moiety was achieved by brief treatment with 10 mM N,N_α-bis(carboxymethyl)-L-lysine in an

* To whom correspondence should be addressed. Phone: 630-252-8298. Fax: 630-252-9151. E-mail: firestone@anl.gov.

† Materials Science Division.

‡ Current address : Cabot Microelectronics, Aurora, IL 60504.

§ Biosciences Division.

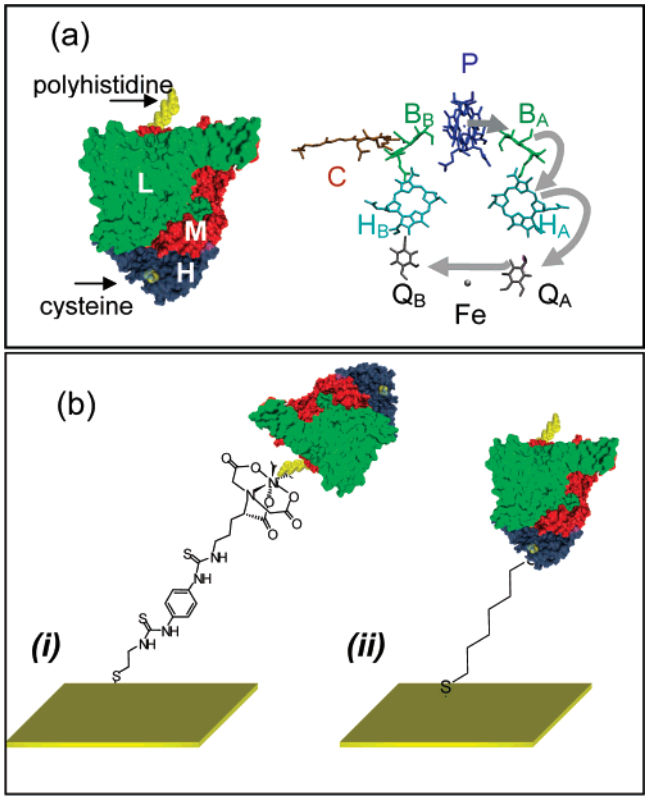

Figure 1. (a) Solid surface representation of a photosynthetic reaction center protein complex (RC) from *R. sphaeroides* and relative position of the cofactor chain buried within the passive polypeptide scaffolding of the RC. (b) Schematic illustration of chemisorption of the RCs onto gold electrodes. (i) On the periplasmic side of the RC, a polyhistidine tag located on the C-terminus of the M subunit is coordinated to a gold surface functionalized with Ni−NTA. (ii) On the cytoplasmic side of the RC, a surface cysteine residue is accessible for disulfide bond formation to a thiohexyl-derviatized gold electrode.

aqueous buffered solution (10 mM potassium phosphate buffer, pH 8). The resulting NTA-functionalized surface was then activated by complexation with Ni^{2+} (20 mM $NiSO_4$), rendering it capable of immobilizing the His-tagged RCs reversibly. The Au−Ni−NTA films were rinsed and stored in 10 mM Tris (pH 8), 0.05% LDAO buffer until RC coupling.

Acceptor-Side Wiring of RCs. Au thin films were incubated in a 0.1 M methanolic solution of 1,6-hexanedithiol for 2 h. For both attachment chemistries, the *R. sphaeroides* RCs were purified as described previously (*7*) and were immobilized by overnight incubation of the functionalized Au films with 0.1 mg/mL RCs in buffered aqueous solution (10 mM Tris (pH 8), 0.05% LDAO) at 4 °C.

Cyclic Voltammetry. Measurements were made on freshly prepared samples in 10 mM Tris (pH 8), 0.05% LDAO buffer using a BAS instruments (West Lafayette, IN) EC Epsilon potentiostat equipped with a C-3 cell stand. The counter electrode was Pt. Ag/AgCl was the reference electrode. Measurements were made on samples in the dark at a range of scan rates (5−20mV/min.) and were performed by scanning from negative to positive potentials. The resulting data were corrected manually to adjust potential values to an NHE electrode.

Atomic Force Microscopy. Atomic force microscopy (AFM) images were acquired under ambient conditions (22 °C, 34−53% relative humidity (RH)) with a SiN cantilever using MultiMode AFM with Nanoscope IV controller and Nanoscope version 5 software (Veeco, Santa Barbara, CA). Conductive AFM (C-AFM) measurements were performed using a MultiMode AFM (Veeco Metrology, Santa Barbara, CA) using Cr−Au coated AFM tips (MikroMasch, Wilsonville, OR). RCs supported on Au-coated microscope slides were mounted on magnetic steel disks and secured on the microscope with electrical contact ensured by Ag paint between the sample and magnetic disk. All imaging was performed in contact mode with a force of 10−15 nN. Samples were imaged with an applied bias of −500 mV and imaged serially in 100 mV increments to a bias of 500 mV. Current−voltage ($I-V$) curves were constructed by measuring current values for individual RCs at each potential.

Scanning Tunneling Spectroscopy. All scanning tunneling spectroscopy (STS) experiments were performed at room temperature using a using MultiMode AFM operating in STM mode (Veeco Metrology) equipped with a Nanoscope IV controller and Pt−Ir probe tips (Veeco). RC samples were mounted on a magnetic steel disk and placed on the microscope. Ag paint was used to ensure electrical contact between the sample and magnetic disk. STS measurements were performed by sampling multiple regions (∼10) of the selected sample. Only data consistent with tip interaction with the chemisorbed RCs were included in the averages. That is, the $I-V$ curves were found to be very sensitive to tip positioning, and accordingly, any data consistent with either poor contact and/or measurement of the underlying organofunctionalized layer were not included in the average. (Data quality was assessed by direct comparison with data collected on a known control, a Ni−NTA-functionalized Au slide). $I-V$ curves were obtained by scanning the sample (at a rate of 1.5 Hz) in forward bias (negative to positive potentials) between −2 and +2 V and then in the reverse direction and averaging the two scans. The absolute tip-to-sample distance is unknown, but all data were collected at a distance where a 200 mV sample bias yields a 1 nA tunneling current. All measurements were made first with the RCs in the dark, shielded from any ambient light using Al foil. The same films were then imaged again after white-light illumination.

Results and Discussion

Two different protein attachment sites, which have been previously used to tether RCs to carbon electrodes (*4*, *8*), were investigated independently in this work. The first attachment site on the protein—a genetically engineered polyhistidine tag (Figure 1a)—is positioned near the periplasmic surface on the C-terminus of the M-subunit. The His-tagged RC complex in its detergent-solubilized (LDAO) form is coupled to a Ni−NTA-functionalized (*9*) gold surface, positioning the RCs such that the primary electron donor, P, is closest to the external electrode surface (Figure 1b(i)). The second attachment site is an accessible cysteine residue (H156Cys) located near the cytoplasmic surface of the H-subunit (Figure 1a). Covalent coupling of the RC at this location serves to position the electron acceptors, Q_A and Q_B ($ubiquinone_{10}$), so that they are oriented closest to the electrode surface (Figure 1b(ii)).

Cyclic voltammetry (CV) was used to verify both electrochemical addressability of the surface-tethered RCs and their asymmetric coupling to the metal electrode. The CV curves collected on RCs immobilized via His-tag coordination to the Ni−NTA-derivatized gold show an irreversible peak with a peak potential of 0.45 V vs Ag/AgCl (or 0.66 V vs NHE; Figure 2a). The position of the primary observed redox event is consistent with the oxidation of the special pair ($P \rightarrow P^+$). The oxidation potential for the special pair has been reported by both electrochemical titrations and voltammetry on RCs in solution or by voltammetry of RCs in thin films, and those methods have yielded values ranging from 0.4 to 0.9 V with

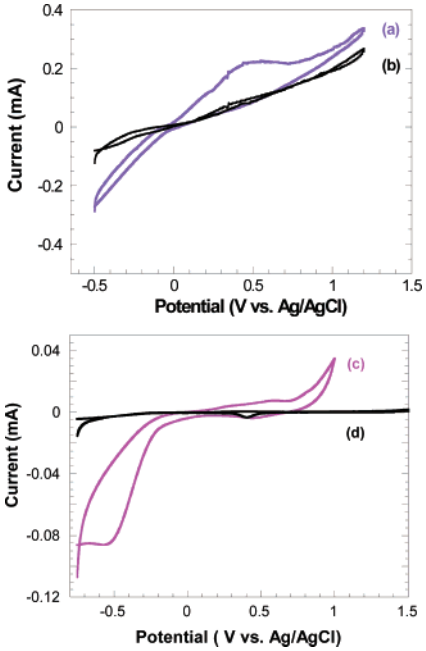

Figure 2. Cyclic voltammograms for (a) polyhistidine-tagged RCs coordinated to Ni−NTA-functionalized gold and (b) the same film after treatment with 1 M imidazole. (c) RCs chemisorbed by disulfide bond formation between a cysteine residue and thiolalkane-derivatized gold and (d) the same film after treatment with 1 M dithionite.

the majority of values occurring at ∼0.5 V (*10*−*12*). The peak potential corresponding to the oxidation of the special pair confirms that the RCs remain electrochemically active and that the RCs are oriented with the periplasmic face in closest proximity to the electrode surface. In addition, a small irreversible shoulder is also noted just below the primary peak (∼0.3 V vs Ag/AgCl; Figure 2a), which may signal the oxidation of the carotenoid (*13*), a cofactor (not in the electron-transfer chain) that functions natively as a photoprotective agent. Similar studies conducted on a carotenoidless strain of RCs (R-26) show near loss of this peak (data not shown). This observation suggests that under these conditions the internal circuit may involve participation of cofactors not involved in the forward physiological electron-transfer chain (i.e., the B-side cofactors including the carotenoid). Continued scans over extended periods of time and at increased scan rates displayed reversible CV peaks, suggesting denaturation of the RCs and possible loss of the redox cofactors (*12*). Further confirmation that the RCs were coordinated to the Ni−NTA-functionalized gold via the polyhistidine tag was obtained when samples were treated with 1 M solutions of imidazole which competes for the Ni−NTA, releasing the RCs from the electrode. The near-complete removal of the RCs was confirmed in CV studies by the loss of the oxidation peak on the imidazole-treated surface (Figure 2b).

Similarly, covalent protein coupling to the accessible cysteine residue at H156 was studied by cyclic voltammetry. The CV recorded for RCs linked to the Au by the formation of a disulfide bond is presented in Figure 2c. The reverse scan shows a single feature positioned at −0.53 V vs Ag/AgCl and corresponds to reduction of the quinones. Most importantly, the irreversible oxidation peak at 0.45 V vs Ag/AgCl is absent, suggesting that the special pair is located far enough away from the electrode surface that it is not oxidized. The observed reduction of the quinone confirms that the RCs remain electrochemically functional when bound at the cysteine location and that the quinone cofactors are in proximity to the electrode surface. As further assurance that the RCs are chemisorbed by disulfide bond

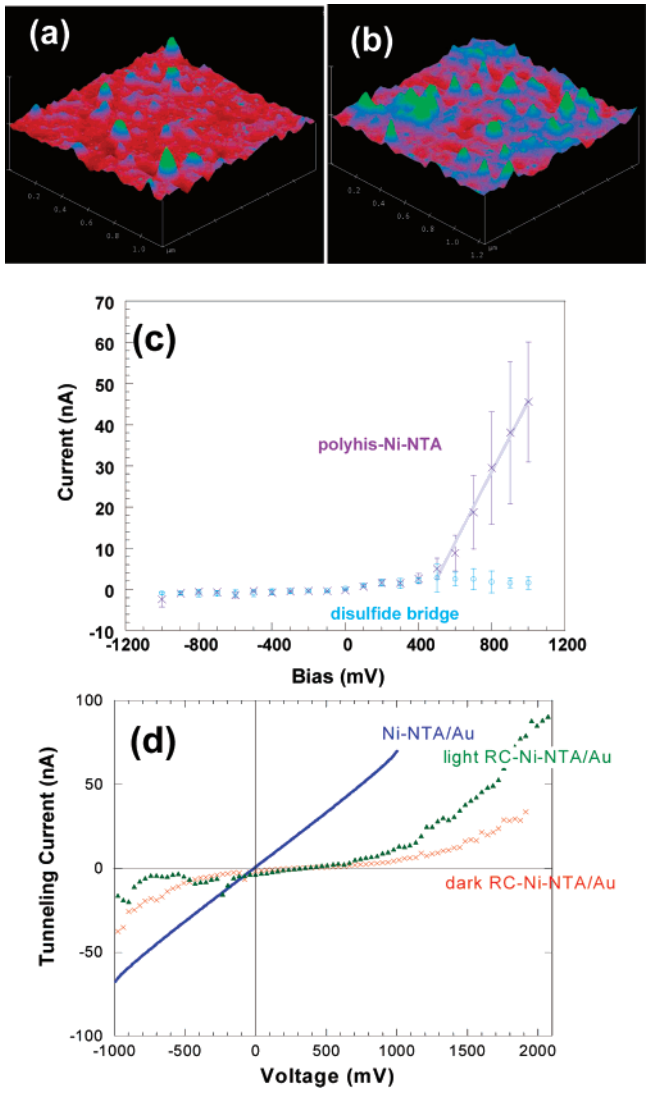

Figure 3. (a) Tapping mode AFM topographic images collected on RCs coordinated to Ni−NTA-functionalized gold electrodes. (b) Tapping mode AFM topographic images collected on RCs chemisorbed to gold electrodes through disulfide bond formation. (c) *I*−*V* curves constructed from C-AFM images of RCs coordinated through the donor side via polyhis−Ni−NTA coupling (purple) and through the acceptor side via disulfide bond formation (blue). (d) Representative *I*−*V* curves determined by STS for the organofunctionalized (Ni−NTA) gold electrodes (blue). Measurements were made with RCs coupled at the donor side via polyhistidine−Ni−NTA at room temperature on dried films, first in the dark (red) and after white-light illumination (green).

formation, the composites were chemically treated with a solution of 1 M $Na_2S_2O_4$ in 10 mM Tris (pH 7.5), 0.05% LDAO which reduces the disulfide bond, cleaving the RCs from the surface (Figure 2d). The liberation of RCs is demonstrated by the featureless voltammogram.

Characterization of individual RCs tethered to gold by the two attachment strategies was also carried out using AFM. A representative AFM image collected for RCs bound to Ni−NTA-derivatized Au via the polyhistidine tag is shown in Figure 3a. The 1 μm × 1 μm image shows six RCs, confirming the low protein surface coverage that is preferable in this work so as to facilitate single-protein transport studies by conductive AFM. A representative AFM image of RCs bound to the gold via disulfide bond formation through the H156 cysteine residue is shown in Figure 3b. The corresponding 1 μm × 1 μm image shows an increased coverage of RCs (14 proteins) relative to polyhistidine−Ni−NTA-coupled RCs. Undoubtedly, the in-

creased protein concentration arises from increased surface coverage of the linker layer, which is expected for the facile, single-step, thiol functionalization of gold.

Electronic transport studies of individual RCs wired to gold electrodes by the two coupling chemistries were carried out by C-AFM. In these studies, a stable two-terminal junction was formed by sandwiching an oriented RC between the electrode and a conductive AFM cantilever. Protein conductance was measured in the dark by current sensing (at the AFM tip) as a function of applied bias (on the gold electrode). $I-V$ curves were constructed by making measurements on at least 10 individual RCs over the full range of biases studied (between -1 V and $+1$ V). The $I-V$ curve measured on individual RCs (identified via imaging mode) bound via polyhistidine coordination to Ni−NTA-derivatized gold (Figure 3c, purple) shows a nonlinear $I-V$ curve with significant asymmetry with respect to the coordinate origin ($V = 0$). The current increases significantly at positive bias and remains invariant (within experimental error) at negative potentials. Furthermore, the $I-V$ curve is essentially linear at positive applied potentials. The global $I-V$ curve, however, exhibits rectification behavior, which is consistent with behavior determined previously for RCs reconstituted into lipid bilayers supported on HOPG electrodes (*14*). Similar $I-V$ curves have also been recorded for photosynthetic proteins derived from plants (photosystem I) and from metalloproteins (*3*, *15*). The observed rectification, which arises from directional electron transfer, here from the gold electrode through the cofactor chain (from P to Q) to the AFM tip, confirms the presence of an oriented RC. The distance between P and the site of attachment (the polyhistidine tag) in this coupling chemistry is difficult to model because the 12 C-terminal residues of the his-tagged M subunit are flexible and, thus, are disordered. The minimum distance between the cytoplasmic surface of the RC and P is 10 Å. The observed transport is consistent with the standard pathway for light-induced chemistry (Figure 1a) and the established fact that the rate for the charge recombination reaction [$(100\ \text{ms})^{-1}$ from $P^+Q_A^-$ or $(1.5\ \text{s})^{-1}$ from $P^+Q_B^-$] is significantly lower than the forward rate [$(200\ \text{ps})^{-1}$ to Q_A or $(100\ \mu\text{s})^{-1}$ to Q_B]. We note, however, that alternative electron-transfer pathways may be operative since oxidation of the carotenoid is observed by voltammetry. Fitting of the linear portion of the ohmic region of the $I-V$ curve yields a resistance of 11.6 MΩ, a value that is significantly less than that determined previously for ferritin and azurin (386 and 660 GΩ, respectively) and is consistent with the enhanced conductivity expected for the RCs (*16*−*18*).

RCs tethered in the opposite orientation via the thiol-coupling chemistry, which positions the H-subunit and the acceptor cofactors (Q_A, Q_B) closest to the Au electrode, yields the $I-V$ curve shown in Figure 3c (blue). The curve is asymmetric but clearly shows a notable reduction in current compared to the Ni−NTA-coupled RCs. The $I-V$ curves observed here compare well with those previously reported for C-AFM studies carried out on self-assembled monolayer thin films carrying physisorbed RCs (*19*). The significant reduction in electron transport observed for RCs bound in this configuration may be attributable to the rather large distance between the site of electrical wiring to the external circuit—at H156Cys—and the internal circuit; the nearest cofactors, Q_A and Q_B, are 30 and 36 Å, respectively, from H156Cys. In addition, the occupancy of the Q_B site in RCs purified with LDAO is only 30% (*20*). When these results are taken together with those of Katz (*8*), who reported conductivity only in Cys-tethered RCs reconstituted with UQ_2 or adsorbed UQ_{10}, they suggest that coupling to the external circuit in RCs tethered at the H156Cys site requires Q_B. Last, it is noted that C-AFM studies of the RCs during white-light illumination cannot be carried out readily by C-AFM due to slow degradation/irreversible photobleaching of the RCs over the time course of the experiment.

Complementary STS studies were conducted on the RCs coupled on the donor side both before and after white-light illumination and the result compared to the $I-V$ curve obtained for a sample without bound protein (Figure 3d). As expected, the $I-V$ curve obtained for samples without RCs show linear (ohmic) response for a metal (Au electrode). The $I-V$ curve collected on RCs in the absence of light shows asymmetry about $V = 0$ and a spectrum similar to that previously reported for RCs derived from higher order plants (PSI and PSII), indicating "diodelike" semiconductor behavior (*21*, *22*). After illumination with white light, the RC spectrum exhibits an increase in tunneling current and the asymmetric component becomes more pronounced (Figure 3d), providing additional evidence that the observed electronic transport is mediated through the protein cofactor chain in the expected fashion. While good reproducibility was found for multiple measurements over the same region, significant variations were observed over the entire film, consistent with the heterogeneous and low surface coverages of the films. A more complete study detailing light-induced conductivity in the RCs is pending, following improved electrical interfacing of the RCs to the electrode.

Conclusions

In summary, we have characterized photosynthetic reaction center proteins interfaced to gold electrodes by two unique protein attachment sites—a genetically introduced polyhistidine tag and a native cysteine residue. Measurements demonstrate that both attachment strategies serve to orient electrochemically active protein unidirectionally on gold electrodes. Single-protein electron transport studies using C-AFM show that RCs wired using polyhistidine coordination to Ni−NTA-functionalized gold display diodelike $I-V$ curves, a result consistent with the known directional electron transport characteristics of the protein. This work also has determined that the native cysteine located on the H-subunit is not suitable for wiring Q_B-depleted RCs to an external circuit and that further work is needed to evaluate this coupling in Q_B-reconstituted RCs and/or to identify an attachment site that is suitable for coupling the external circuit to Q_A and the A-branch cofactors. Future work will focus on protein engineering to introduce a unique attachment site closer to the acceptor cofactors for improved electron transport. In addition, further studies will be directed at optimizing current flow in the RC−electrode composites by tuning the metal−organic interface, including adjustment of protein orientation, shortening the linker (wire), and changing the chemical composition of the linker. This work, however, represents a first step toward identifying means by which biologically active components can be integrated with inorganic device materials to create bio-optoelectronic materials and devices.

Acknowledgment

This work was supported by the United States Department of Energy under Contract No. DE-AC02-06CH11357 to the UChicago, LLC.

References and Notes

(1) Laible, P. D.; Kelley, R. F.; Wasielewski, M. R.; Firestone, M. A. Electron-transfer dynamics of photosynthetic reaction centers in

thermoresponsive soft materials. *J. Phys. Chem. B* **2005**, *109*, 23679−23686.
(2) Lu, Y.; et al. Manipulated photocurrent generation from pigment-exchanged photosynthetic proteins adsorbed to nanostructured WO_3−TiO_2 electrodes. *Chem. Commun. (Cambridge)* **2006**, 785−787.
(3) Lee, I.; Lee, J. W.; Greenbaum, E. Biomolecular electronics: Vectorial arrays of photosynthetic reaction centers. *Phys. Rev. Lett.* **1997**, *79*, 3294−3297.
(4) Das, R.; et al. Integration of photosynthetic protein molecular complexes in solid-state electronic devices. *Nano Lett.* **2004**, *4*, 1079−1083.
(5) Inagaki, S.; Guan, S.; Fukushima, Y.; Ohsuna, T.; Terasaki, O. Novel mesoporous materials with a uniform distribution of organic groups and inorganic oxide in their frameworks. *J. Am. Chem. Soc.* **1999**, *121*, 9611−9614.
(6) Deisenhofer, J.; Epp, O.; Miki, K.; Huber, R.; Michel, H. Structure of the protein subunits in the photosynthetic reaction center of rhodopseudomonas-viridis at 3Å resolution. *Nature* **1985**, *318*, 618−624.
(7) Pokkuluri, P. R.; et al. The structure of a mutant photosynthetic reaction center shows unexpected changes in main chain orientations and quinone position. *Biochemistry* **2001**, *41*, 5998−6007.
(8) Katz, E. Application of bifunctional reagents for immobilization of proteins on a carbon electrode surface: Oriented immobilization of photosynthetic reaction centers. *J. Electroanal. Chem.* **1994**, *365*, 157−164.
(9) Hochuli, E.; Dobeli, H.; Schacher, A. New metal chelate adsorbent selective for proteins and peptides containing neighboring histidine-residues. *J. Chromatogr.* **1987**, *411*, 177−184.
(10) Lin, X.; et al. Specific alteration of the oxidation potential of the electron-donor in reaction centers from Rhodobacter-Sphaeroides. *Proc. Natl. Acad. Sci. U.S.A.* **1994**, *91*, 10265−10269.
(11) Geskes, C.; Meyer, M.; Fischer, M.; Scheer, H.; Heinze, J. Electrochemical investigation of modified photosynthetic pigments. *J. Phys. Chem.* **1995**, *99*, 17669−17672.
(12) Munge, B.; Pendon, Z.; Frank, H. A.; Rusling, J. F. Electrochemical reactions of redox cofactors in *Rhodobacter sphaeroides* reaction center proteins in lipid films. *Bioelectrochemistry* **2001**, *54*, 145−150.
(13) He, Z. F.; Kispert, L. D. Electrochemical and optical study of carotenoids in TX100 micelles: Electron transfer and a large blue shift. *J. Phys. Chem. B* **1999**, *103*, 9038−9043.
(14) Stamouli, A.; Frenken, J. W. M.; Oosterkamp, T. H.; Cogdell, R. J.; Aartsma, T. J. The electron conduction of photosynthetic protein complexes embedded in a membrane. *FEBS Lett.* **2004**, *560*, 109−114.
(15) Rinaldi, R.; et al. Electronic rectification in protein devices. *Appl. Phys. Lett.* **2003**, *82*, 472−474.
(16) Xu, D.; Watt, G. D.; Harb, J. N.; Davis, R. C. Electrical conductivity of ferritin proteins by conductive AFM. *Nano Lett.* **2005**, *5*, 571−577.
(17) Huang, Y. W.; Zhao, Y. Y. *Appl. Phys. Lett.* **2004**, *84*, 2028−2030.
(18) Alessandrini, A.; Salerno, M.; Frabboni, S.; Facci, P. Single-metalloprotein wet biotransistor. *Appl. Phys. Lett.* **2005**, *86*.
(19) Mikayama, T.; Miyashita, T.; Iida, K.; Suemori, Y.; Nango, M. Electron transfer mediated by photosynthetic reaction center proteins between two chemical-modified metal electrodes. *Mol. Cryst. Liq. Cryst.* **2006**, *445*, 291−296.
(20) Laible, P. D.; et al. Quinone reduction via secondary B-branch electron transfer in mutant bacterial reaction centers. *Biochemistry* **2003**, *42*, 1718−1730.
(21) Lee, I.; Lee, J. W.; Warmack, R. J.; Allison, D. P.; Greenbaum, E. Molecular electronics of a single photosystem-I reaction-center—Studies with scanning-tunneling-microscopy and spectroscopy. *Proc. Natl. Acad. Sci. U.S.A.* **1995**, *92*, 1965−1969.
(22) Lukins, P. B.; Oates, T. Single-molecule high-resolution structure and electron conduction of photosystem II from scanning tunneling microscopy and spectroscopy. *Biochim. Biophys. Acta (Bioenergetics)* **1998**, *1409*, 1−11.

Received February 5, 2007. Accepted June 6, 2007.

BP070042S